# Exploring Western North Pacific Tropical Cyclone Activity in the High-Resolution Community Atmosphere Model

**Xiaoning Wu[1], Kevin A. Reed[1], Patrick Callaghan[2], Julio T. Bacmeister[2]**

[1]School of Marine and Atmospheric Sciences, Stony Brook University, Stony Brook, NY
[2]Climate and Global Dynamics Laboratory, National Center for Atmospheric Research, Boulder, CO

**Key Points:**

- In TC-permitting CAM5, cold and dry biases over Pacific Warm Pool leads to lack of WNP TCs
- Constraining WNP large-scale environment by nudging temperature improves Warm Pool convection and TCs
- TC genesis and intensity development are sensitive to the choice of nudging timescale

Corresponding author: Xiaoning Wu, xiaoning.wu.1@stonybrook.edu

## Abstract

High-resolution climate models (∼28 km grid spacing) can permit realistic simulations of tropical cyclones (TCs), thus enabling their investigation in relation to the climate system. On the global scale, previous works have demonstrated that the Community Atmosphere Model (CAM) version 5 presents a reasonable TC climatology under prescribed present-day (1980-2005) forcing. However, for the Western North Pacific (WNP) region, known biases in simulated TC genesis frequency and location under-represent the basin's dominant share in observation. This study addresses these model biases in WNP by evaluating WNP TCs in a decadal simulation, and exploring potential improvements through nudging experiments. Among the major environmental controls of TC genesis, the lack of mid-level moisture is identified as the leading cause of the deficit in simulated WNP TC genesis over the Pacific Warm Pool. Subsequent seasonal experiments explore the effect of constraining the large-scale environment on TC development by nudging WNP temperature field towards reanalysis at various strengths. Temperature nudging elicits significant response in TC genesis and intensity development, as well as in moisture and convection over the Warm Pool. These responses are sensitive to the choice of nudging timescale. Overall, the nudging experiments demonstrate that improvements in the large-scale environment can lead to improvements in simulated TCs. The verification of the environmental controls for simulated TC genesis suggests future model developments in relation to model physics. The potential improvements will contribute to the understanding of how the mean state of current or future climates may give rise to extremes such as TCs.


## 1 Introduction

Tropical cyclones (TCs), an extreme form of organized deep convection, typically have a horizontal spatial scale on the order of ∼1000 km. The potentially severe societal impacts of these weather events add to the motivation for their investigation under current and future climates (e.g., Bakkensen & Mendelsohn, 2019). With computational advances, high-resolution general circulation models (GCMs), with horizontal grid spacing finer than 50 km, permit the explicit simulation of TCs as a part of the global climate system (Zhao et al., 2009; Shaevitz et al., 2014; Bacmeister et al., 2014; Murakami et al., 2015; K. Reed et al., 2015; Walsh et al., 2015; Bacmeister et al., 2018; Stansfield et al., 2020). Many of these TC-permitting GCMs present a fairly realistic global clima-

tology of TC tracks, although model-specific biases often emerge at the basin scale (e.g. Wehner et al., 2017; Camargo et al., 2020; Roberts et al., 2020). For example, the Community Atmosphere Model version 5 (CAM5) with a horizontal grid spacing of ∼28 km simulates a reasonable TC distribution at the global scale, but regional biases in TC genesis frequency and location persist across different configurations, especially for the Western North Pacific (WNP) basin (Bacmeister et al., 2014; Wehner et al., 2014; K. Reed et al., 2015; Bacmeister et al., 2018). These biases underrepresent the basin's share in global TC climatology, complicating the interpretation of future projections on both regional and global scales.

These model- and region-specific biases in simulated TCs are often linked to the mean state of the surrounding large-scale environment, in particular the thermodynamic and dynamic conditions affecting TC genesis and development. Of these, ocean coupling have been shown to improve TC intensity development via air-sea fluxes (Ogata et al., 2015; H. Li & Sriver, 2018; Scoccimarro et al., 2017). Notably, H. Li and Sriver (2018) also discussed improvement in convection over the Pacific Warm Pool with slab and dynamic ocean coupling. For the atmospheric component, a well-known sensitivity for simulated TCs in GCMs is the choice of convective parameterization (K. A. Reed & Jablonowski, 2011; Zhao et al., 2012; Zarzycki & Jablonowski, 2015; Wehner et al., 2017). More specifically, Wehner et al. (2014) discussed the representation of extreme precipitation and TCs in high-resolution CAM5. While the high tail-end of precipitation distribution is better represented at TC-permitting resolutions, the mean precipitation climatology degraded relative to the standard lower resolution (Bacmeister et al., 2014). These analyses raise the question of the relationship between the simulated mean state of the convective environment and TCs on the extreme end.

To identify the linkages between the large-scale environment and simulation features, nudging is a helpful technique which relaxes the simulation towards observation (Haseler, 1982; Klinker, 1990). Previous studies have explored the effects of nudging on regional TC simulation, including the western North Pacific (Feser & Barcikowska, 2012; Choi & Lee, 2016; Barcikowska et al., 2017; Moon et al., 2018), the North Atlantic (Knutson et al., 2007), and the Bay of Bengal (Yesubabu et al., 2014). In cases where the large-scale winds are the target of constraint, spectral nudging (e.g. von Storch et al., 2000) is implemented on the wind field only, at spatial scales greater than that of TCs (e.g. Feser & Barcikowska, 2012; Wang et al., 2013; Choi & Lee, 2016; Barcikowska et al., 2017).

On the other hand, when multiple state variables – velocity, temperature, and humidity – are nudged, the respective roles of dynamic and thermodynamic factors on the model behavior often merit further study (Knutson et al., 2007).

In this study, we explore this question: Does improved simulation of the large-scale mean environment lead to improved simulation of TCs in high-resolution CAM5? We first evaluate the 1980-2005 decadal climatology of simulated TCs in CAM5 in detail over WNP. Biases are identified in the mean state of the large-scale environment that are responsible for the biases in simulated TCs. Subsequently we carry out additional seasonal simulation experiments to address these mean-state biases, with and without nudging relevant state variables towards observation. Section 2 details the data, methods and experimental design. Section 3 presents the results. Finally, Section 4 discusses the conclusions and further research.

## 2 Data and Methods

### 2.1 Community Atmosphere Model version 5, and the Decadal Experiment

The model simulations use CAM5, fully described in Neale et al. (2012). The model physics consist of a moist turbulence scheme (Bretherton & Park, 2009), shallow convection scheme (Park & Bretherton, 2009), deep convection (G. J. Zhang and McFarlane (1995) with modifications, see Neale et al. (2012) for details), cloud microphysics (Gettelman et al., 2008), and other components. The modal aerosol model is implemented with prognostic aerosols (Easter et al., 2004).

Both the decadal and seasonal simulations are configured with the finite-volume dynamical core at 0.25° horizontal resolution. The boundary condition and other forcing follow the protocols of the Atmospheric Model Intercomparison Project (AMIP; see Gates, 1992; Gates et al., 1999), with prescribed sea surface temperature, sea ice, and greenhouse gases. The setup of the decadal simulation is further described in K. Reed et al. (2015). High-resolution CAM5 (at 0.25° horizontal resolution) has been extensively used and evaluated for TC simulation under various AMIP configurations (Wehner et al., 2014; Bacmeister et al., 2014; K. Reed et al., 2015; Zarzycki & Jablonowski, 2015; Zarzycki, 2016; K. A. Reed et al., 2019).

### 2.2 The Seasonal Experiments and Method for Nudging

The nudging toolbox in the Community Earth System Model framework provides a platform for model testing (NCAR, 2017). This module provides an extra forcing term for model prognostic variables (temperature, specific humidity, U- and V-wind), driving them towards a prescribed state often derived from reanalyses, while the rest of the model operates as in free run. The forcing term is typically in the following form, in the example of temperature ($T$):

$$\dot{T_{ndg}} = C(x,y,z)\frac{T_{model}(t) - T_{ana}(t)}{\tau}, 0 \leq C \leq 1 \tag{1}$$

where $C$ is a coefficient that specifies the three-dimensional coverage and strength of nudging. The nudging timescale ($\tau$) is typically set to six hours, synchronizing with the temporal resolution of reanalysis data. Reducing $C$ is equivalent to relaxing the nudging timescale and reducing the strength of nudging.

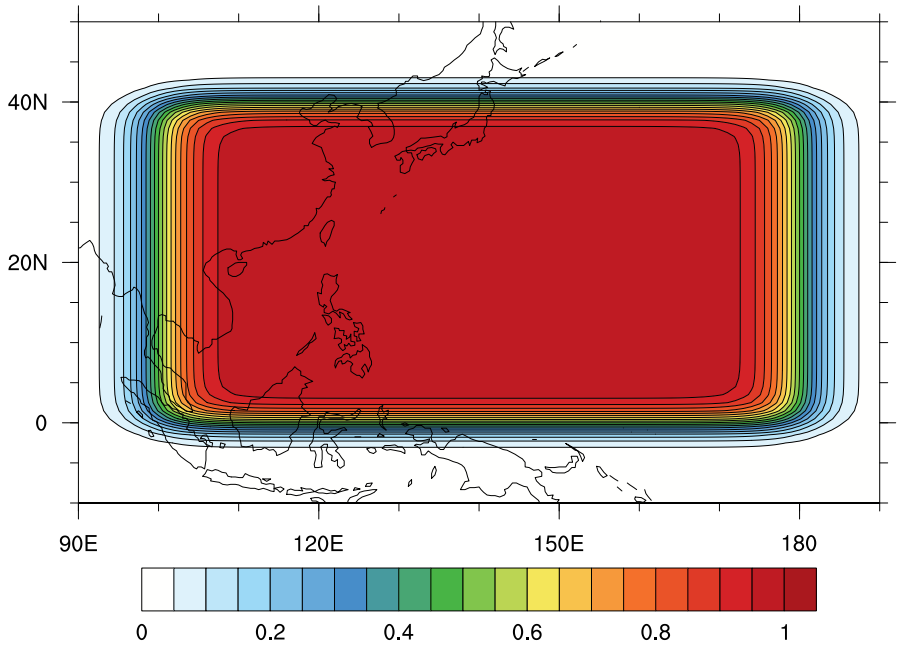


**Figure 1.** The value of $C$ used for the nudging experiments, showing the horizontal coverage on all vertical levels.

The seasonal experiments with nudging are motivated by the biases in the large-scale mean state connected to the biases in simulated TCs from the free-running decadal simulation, discussed in Section 3.1. Based on the cold and dry biases we find in the decadal simulation, we have chosen to nudge the temperature, with the expectation that the biases in specific humidity ($q$) will also be reduced when the temperature is constrained. The impact of directly nudging specific humidity instead is briefly discussed in Section 4. These seasonal experiments are conducted for 1993, an ENSO-neutral year with an average number of WNP TCs, to avoid the impact of El Niño or La Niña years on the seasonal climatology of WNP TCs. The temperature field from ERA-Interim (Dee et al., 2011) is preprocessed onto CAM5 grids for the nudging experiments. We explore the effect of temperature nudging on WNP large-scale environment and subsequent TC genesis with a range of nudging strength: CTRL case (no nudging), T(0.125) case (1/8 nudging strength, $\tau = 48$h), T(0.5) case (1/2 nudging strength, $\tau = 12$h), and T(full) case (full nudging, $\tau = 6$h). Each case comprises of five ensemble runs. For each run, the simulation is initialized from ERA-Interim on April 1st, 1993, and ran through October with their respective nudging strength. The analysis focuses on July-October (JASO), the peak season for WNP TCs. The same nudging window (Fig. 1) is implemented across all three nudging cases, covering WNP in the horizontal and invariant in the vertical. In a supplementary set of experiments, only the vertical levels above 850 hPa are nudged to allow free evolution of the lower levels. This does not qualitatively change the results from all-level nudging. Except the nudging, the CAM5 setup for the seasonal experiment is otherwise identical with the decadal simulation.

### 2.3 Validation and Diagnostics

Observed TC tracks are taken from the International Best Track Archive for Climate Stewardship (IBTrACS; Knapp et al., 2010), and all TCs from the WNP basin are included in the comparison to simulation. Simulated TCs from both the decadal and seasonal experiments are tracked from three-hourly model outputs by the TempestExtremes package (Ullrich & Zarzycki, 2016), based on threshold criteria of minimum sea level pressure, maximum wind speed, a warm core, and duration of persistence. Sensitivity of the tracking criteria is discussed by Zarzycki and Ullrich (2017), and we find that the results of this study concerning simulated TC tracks are robust over a number of available track-

ing methods, including that from Zhao et al. (2009), as well as various options for warm core detection in Zarzycki and Ullrich (2017).

To evaluate the large-scale environment of CAM5 simulations, ERA-Interim (Dee et al., 2011) and Modern-Era Retrospective analysis for Research and Applications Version 2 (MERRA2; Gelaro et al., 2017) are used for the thermodynamic and dynamic fields. Specifically, the moisture fields are discussed by Berrisford et al. (2011) for ERA-Interim, and Bosilovich et al. (2017) for MERRA2. In addition, the global precipitation climatology project (GPCP; Adler et al., 2003) dataset is used for precipitation, and NOAA's Climate Data Record (CDR; Lee, 2014) is used for outgoing longwave radiation.

To inspect the simulated large-scale environment in relation to the genesis of TCs, genesis potential index (GPI, see Emanuel, 2010) is calculated from the monthly fields of CAM5 simulations and reanalyses. The GPI is based on an empirical relationship between TC genesis and four large-scale environmental controls: low-level (850 hPa) absolute vorticity ($\eta$), mid-level (600 hPa) moist entropy deficit ($\chi$), TC potential intensity (PI; see Bister & Emanuel, 2002), and vertical wind shear (VWS):

$$GPI \equiv |\eta|^3 \chi^{-4/3} MAX[(PI - 35ms^{-1}), 0]^2 (25ms^{-1} + VWS)^{-4} \tag{2}$$

where moist entropy deficit ($\chi$) and moist entropy ($s$) are defined as follows (Emanuel et al., 2008):

$$\chi \equiv \frac{s^*_{mid} - s_{mid}}{s^*_{surface} - s^*_{mid}} \tag{3}$$

$$s \equiv c_p lnT - R_d lnp + \frac{L_v q}{T} - R_v q lnRH \tag{4}$$

In Eq. 3, $s^*$ represents saturation moist entropy at the specified pressure level. In Eq. 4, $c_p$ is the heat capacity of dry air, $R_d$ is the gas constant of dry air, $p$ is pressure, $L_v$ is the latent heat of vaporization following Bryan (2008), $R_v$ is the gas constant of water vapor, and $RH$ is relative humidity. As a metric of mid-level moisture, moist entropy deficit ($\chi$) is closely related to relative humidity, which was used in a previous formulation of GPI (Emanuel & Nolan, 2004).

For the statistical diagnosis, pairwise statistical distances between the CAM5 experiments and the observed records are calculated using the Z-statistics from the two-sided Kolmogorov-Smirnov test (see Eq. 5.17–18 from Wilks, 2011):

$$Z_s \equiv (\frac{n_1 n_2}{n_1 + n_2} MAX|F(x_1) - F(x_2)|)^{1/2} \tag{5}$$

where $n_1$ and $n_2$ are the sample sizes, and $F(x_1)$ and $F(x_2)$ are the empirical cumulative distribution functions (CDF).

## 3 Results

### 3.1 WNP TC Genesis in CAM5 Decadal Simulation (1980-2005)

In the CAM5 decadal simulation, WNP TC genesis is biased in both location and frequency, which subsequently affect track intensity development. Fig. 2 shows WNP TC tracks and intensity from observation and the decadal simulation of the peak season (July-October), which have included TCs that developed east of 180° E and moved into the basin. As identified by previous studies (Bacmeister et al., 2014; Wehner et al., 2014; K. Reed et al., 2015), the simulated WNP TC frequency is lower than observation by 45%. Moreover, the lack of TC genesis in the lower latitudes (near absence south of 10° N) in the CAM5 decadal simulation leads to biases in the spatial pattern of TC intensity development. As simulated TCs form at higher latitudes than in observation, the latitudes at which they mature in intensity show a corresponding shift to the north, from about 20° N in observation to about 30° N in simulation. These biases would negatively affect the representation of landfalling statistics, as well as TC-induced extreme precipitation over land.

The climatology of simulated GPI reflects the biases in simulated TC genesis (Fig. 3). Note that by only keeping TCs formed in WNP, the simulated TC frequency is further reduced from Fig. 2. In observation (Fig. 3, middle column), the area of high GPI south of 20° N inside the Warm Pool corresponds well to the main development region seen in TC genesis density. In the CAM5 simulation (Fig. 3, left column), while the spatial patterns of TC genesis and GPI show comparable agreement, the centers of both are shifted north of 20° N, out of the Warm Pool. This northward bias is further reflected in the right column of Fig. 3, showing the CAM5-to-observation ratio for TC genesis and

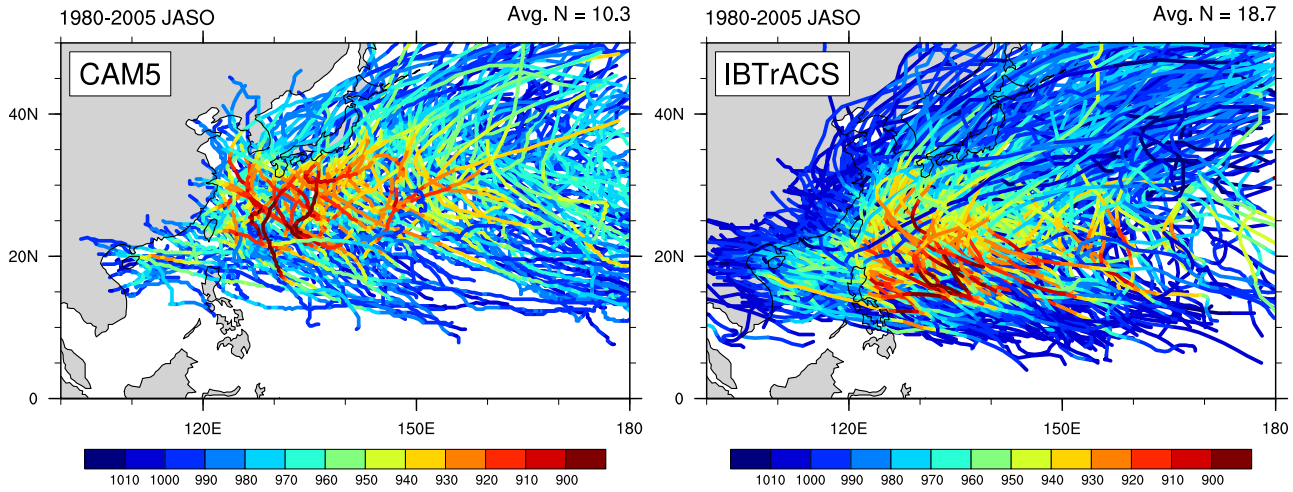


**Figure 2.** WNP TC tracks and intensity from observation and CAM5 decadal simulation, July-October 1980-2005. The annual average number of TC genesis within the season is shown in the upper right corner.

GPI; in the CAM5 simulation, both TC genesis and GPI are lacking over the Warm Pool. Repeating the comparison with observed GPI from MERRA2 (not shown) results in consistent patterns. The consistency between simulated GPI and TC genesis suggests that the large-scale environmental controls comprising GPI may help to explain the underlying causes for the biases in TC genesis.

The contribution to the biases in GPI (Eq. 2) from each components is decomposed in Fig. 4, showing the lack of mid-level moisture in the Warm Pool as the leading cause of the deficit in GPI in the CAM5 simulation. The overestimation of mid-level moist entropy deficit is responsible for the underestimation of GPI over the Warm Pool. While the lack of relative vorticity also reduces GPI in the main develop region south of 20° N, its contribution to the bias is smaller in magnitude and less spatially expansive. Potential intensity is generally overestimated in the CAM5 simulation, and vertical wind shear generally introduces the smallest bias in GPI. Repeating the decomposition with observed GPI from MERRA2, the bias due to mid-level moist entropy deficit is even more outstanding over the Warm Pool, while the other three GPI components remain qual-

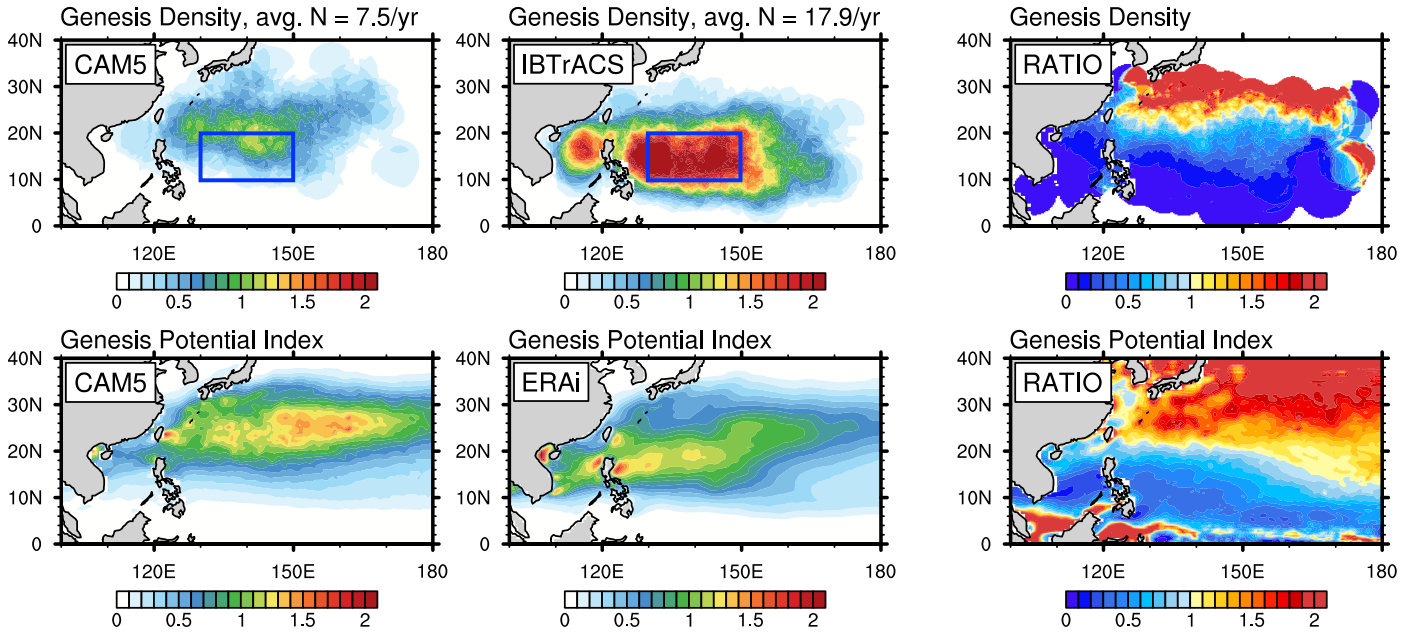


**Figure 3.** Top row: Area-weighted TC genesis density (over a 5° radius) of July-October 1980-2005, from observation and CAM5 simulation. Bottom row: Corresponding GPI, scaled by a constant uniform coefficient to match the magnitude of TC genesis density. The ratio is calculated by dividing CAM5 simulation by observation (blue: underestimation in CAM5, red: overestimation in CAM5). The blue box (10-20°N, 130-150°E), encompassing 60% of observed TC genesis, is further examined in Fig. 5 and 9.

itatively similar (not shown). In the interest of diagnosing model biases and exploring potential improvements for WNP TC genesis, the dominance of the moist entropy deficit component in GPI bias prompts a focused investigation of the biases in Warm Pool moisture and the potential impact on simulated TCs.

Focusing on the main development region of 10-20°N, 130-150°E (the blue boxes in Fig. 3), which encompasses the hot spots of TC genesis in observation, a comparison of the vertical profiles of temperature and humidity reveals cold and dry biases over this region (Fig. 5). The temperature and humidity fields both contribute to the difference in moist entropy deficit (Eq. 3 and 4). Fig. 5(a), (c), and (d) show the difference between the CAM5 simulation and ERA-Interim reanalysis, with MERRA2 also plotted for reference. For the temperature profile (Fig. 5(a)), while CAM5 falls in between the two reanalyses close to the surface, the cold bias grows throughout the higher levels, reaching

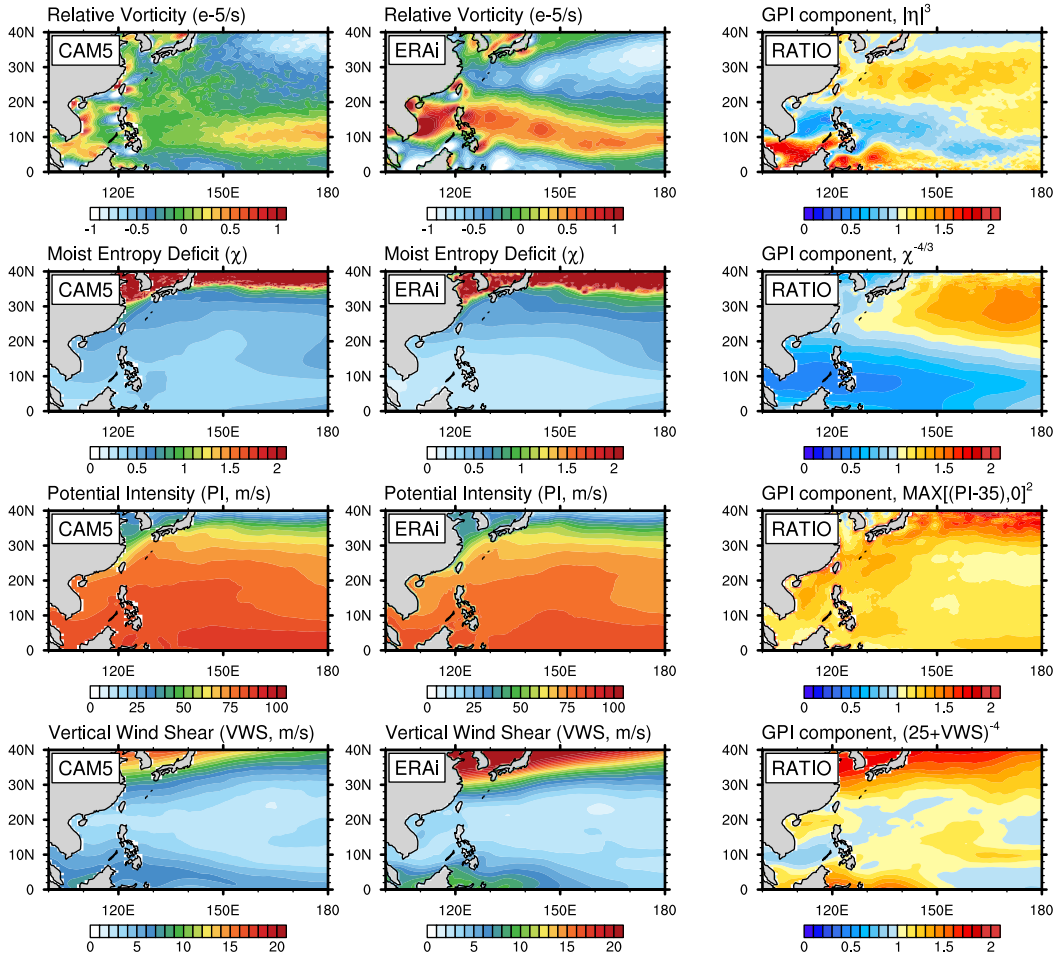


**Figure 4.** The four environmental variables comprising GPI, and their respective contribution to GPI bias in the simulation by ratio, July-October 1980-2005. Note that while the first two columns are showing the values of the variables, the ratio as in Fig. 3 is calculated over the corresponding GPI component, e.g. $\chi^{-4/3}$ for moist entropy deficit.

about 1 K at the mid-levels when compared to ERA-Interim. This leads to the corresponding pattern in the profile of saturation specific humidity (Fig. 5(c)). For specific humidity (Fig. 5(d)), while CAM5 behaves more MERRA2-like at the low levels below 900 hPa, a dry bias exists and is largest at about 800 hPa, and persists throughout the higher levels. MERRA2 has more mid-level moisture in this region than ERA-Interim in terms of both specific and relative humidity (Fig. 5(b)), consistent with the more outstanding bias from the moisture entropy deficit term when using MERRA2 for the GPI decomposition in Fig. 4 (not shown). For CAM5, Fig. 5(b) shows that while the saturation specific humidity is slightly reduced due to the cold bias, the pronounced lack of

specific humidity relative to the two reanalyses leads to excessive moisture entropy deficit, as seen in Fig. 4.

The cold and dry biases that extend over the Warm Pool (first and second rows in Fig. 6) are potentially linked to known deficits in the convective environment. The third row of Fig. 6 shows a comparison of the large-scale flow on the mid-level between CAM5 and ERA-Interim over the WNP region. ERA-Interim shows a clear pattern of East Asian Summer Monsoon circulation over the western side of the WNP. The spatial extent of the monsoon trough is associated with the large-scale environment for WNP TC development through both humidity and dynamics, as discussed by observation-based (Sadler, 1976; L. Wu et al., 2012) and modeling studies (L. Wu et al., 2014; Murakami et al., 2011). In CAM5, the flow around the Philippines is lacking the recurvature as seen in the reanalysis, contributing to the lack of horizontal convergence over the Warm Pool. Combined with a lack of humidity (Fig. 6, second row), the resulting lack of moisture flux convergence (Fig. 6, third row) reflects the precipitation deficit (Fig. 6, fourth row) discussed by Bacmeister et al. (2014). Another feature related to the lack of convection in CAM5 is the surplus of outgoing longwave radiation (Fig. 6, bottom row), partly due to the lack of deep convection and high clouds over the Warm Pool (Sobel & Camargo, 2005; L. Wu et al., 2012). The resulting effect on the energy budget may have contributed to the cold bias.

In this section, we have examined the climatology of WNP TC genesis in the CAM5 decadal simulation, in relation to the cold and dry biases in the large-scale environment over the Warm Pool. While a detailed explanation of the large-scale biases is beyond the scope of this study, we hypothesize that improving the large-scale environment will improve TC genesis. Specifically, correcting the biases in temperature and moisture over the Warm Pool may lead to more realistic TC genesis in this region. In the next section, we bring this hypothesis to test by conducting a suite of simulation experiments with temperature nudging.

### 3.2 Seasonal Experiments (1993) with Temperature Nudging

In the previous section, we have identified the lack of mid-level moisture, connected to the overall cold and dry biases over the WNP Warm Pool, as the leading cause of the biases in simulated TCs. To explore the improvement of this cold and dry bias and its

potential impact on simulated TCs, we conducted seasonal simulation experiments nudging the temperature field towards reanalysis with a range of strengths (see Section 2.2). As shown in Fig. 7, reducing the bias in temperature by nudging has a pronounced effect on TC genesis and subsequent development. As expected, the CTRL case shows similar biases as the previously discussed decadal simulation (Fig. 2), with TC genesis and tracks shifted to the north of the Warm Pool. As the strength of nudging increases, TC genesis migrates south into the Warm Pool, increasingly consistent with observation. At the same time, TC intensity development is increasingly dampened by the strength of nudging, presumably due to the interference of the nudging term with the evolution of TCs' structure. On the other hand, the improvement in TC genesis location potentially allows TC tracks to more realistically develop and interact with other large-scale systems, such as the Western Pacific Subtropical High (George & Gray, 1977; Camargo et al., 2007; W. Zhang et al., 2013b). The recurvature and intensification of TCs typically observed in this region affects track development as well as landfalling statistics over East Asia (Camargo et al., 2007; W. Zhang et al., 2013a). This effect is more readily seen in the relaxed nudging cases, T(0.125) and T(0.5), where more TC tracks recurve while intensifying compared to the CTRL case.

The improvements in TC genesis in the nudging cases are consistent with GPI, with major contribution from the moist entropy component (Fig. 8). For the CTRL case, GPI and its components (not shown) are similar to the previously analyzed decadal climatology. We note that even in the T(full) case, the response of moisture does not align perfectly with the reanalysis. Nevertheless, all the nudging cases show a marked decrease in mid-level moist entropy deficit over the Warm Pool, thus decreasing this term's contribution to the bias in GPI, and improving the pattern of GPI over the basin. Meanwhile, the relative bias contribution by the other three components of GPI (not shown) are not substantially affected. Curiously, the response of mid-level moist entropy deficit to the strength of nudging is not monotonic. Specifically, as more easily seen in the bottom row of Fig. 8, mid-level moist entropy deficit increased east of the Philippines in T(full) compared to both T(0.5) and T(0.125), causing a reduction in GPI.

A closer inspection of the vertical structure of temperature and moisture responses to nudging (Fig. 9) helps to explain their combined effect on GPI. For the CTRL case, the cold (Fig. 9(a) and Fig. 9(c)) and dry (Fig. 9(d)) biases are consistent with that of the decadal simulation shown in Fig. 5. We notice that due to the complexities of model

physics, the temperature field from the T(full) case does not exactly replicate the reanalysis. Nevertheless, in all the nudging cases, the temperature profiles show a clear and systematic reduction of the cold bias corresponding to the strength of nudging (Fig. 9(a)). Saturation specific humidity (Fig. 9 (b) and (c)) follows the temperature field correspondingly. Specific humidity (Fig. 9 (b) and (d)), while responding somewhat non-monotonically to the strength of nudging, shows marked improvement to the dry bias above the boundary layer. At the mid-level, all three nudging cases (T(0.125), T(0.5) and T(full)) are much closer to ERA-Interim in specific humidity (Fig. 9 (d)) than the overly dry CTRL case. Focusing on the 600 hPa level, we observe that compared to T(0.5) and T(0.125), T(full) is both warmer and dryer (Fig. 9 (c) and (d)), thus having a lower relative humidity and higher moist entropy deficit, in explanation of the previously discussed patterns in Fig. 8. We note that at the lower levels, temperature nudging may lead to drying, most pronounced in the T(full) case (Fig. 9 (d)). Overall, while there are subtleties in the responses of temperature and moisture across the nudging cases at different levels, temperature nudging can improve both the cold and dry biases, particularly above the boundary layer.

The spatial patterns of the response of temperature, moisture, and precipitation over the Warm Pool (Fig. 10) are consistent with the relationships discussed above. As seen in the vertical profiles (Fig. 9), while 600 hPa temperature fields from the nudging cases become closer to the reanalysis with increasing strength of nudging, the specific humidity field of T(full) drops below that of T(0.5). This increase in the dry bias from T(0.5) to T(full) is possibly due to the over-reaction of convective activities in T(full), evident in excessive precipitation (Fig. 10, bottom row). The T(0.125) case also shows an increase in precipitation in the WNP region from CTRL, but not nearly as much as in the T(0.5) and T(full) cases, and still has much lower precipitation in the Warm Pool compared to GPCP. To summarize the responses of other aspects of circulation and convection discussed for the decadal simulation in Fig. 6, both T(0.5) and T(full) are qualitatively closer to observation than T(0.125). For the East Asian Summer Monsoon (not shown), while both T(0.5) and T(full) substantially improved the representation of the monsoon trough discussed in Section 3.1, T(0.125) falls closer to the biased CTRL case. Combined with a lack of specific humidity, the bias in moisture flux convergence of T(0.125) coincides with deficits in Warm Pool precipitation, similar to the CTRL case. In all three nudging cases, the response of outgoing longwave radiation largely follows that of pre-

cipitation, suggesting substantial contribution from convective high clouds. Overall, these responses in the large-scale environmental factors to various strengths of temperature nudging are consistent with, and coupled to, the responses of simulated TCs shown in Fig. 7.

### 3.3 Statistics of WNP TC Response to Temperature Nudging

With the responses of the large-scale environment in mind, we return to the simulated TCs for a statistical evaluation on the impact and limitations of temperature nudging over various timescales. As previously observed in Fig. 7, temperature nudging affects TCs for both genesis and the spatial characteristics of intensity development. The CDFs (Fig. 11) provide an overview of the meridional distributions of TC genesis and lifetime maximum intensity, across all CAM5 cases and the decadal and seasonal samples from observation. For TC genesis, the CDF confirms the incremental migration towards observation as nudging strength increases, consistent with GPI (Fig. 8). For TC lifetime maximum intensity, however, while the CDFs likewise migrate southwards, TCs from the T(full) case overshoot observation by reaching their lifetime maximum intensity too close to genesis, likely linked to the reduction in TC intensity (Fig. 7) by full-strength nudging towards the state from reanalysis.

In addition to the CDFs, Fig. 12 shows the Z-statistics from the two-sided Kolmogorov-Smirnov test as introduced in Section 2.3. The value of Z-statistics adjusts the maximum difference between any given pair of CDFs shown in Fig. 11 by the sample sizes of the pair under comparison, where lower values of Z-statistics correspond to lower confidence in the statistical difference between the two samples. To confirm the justification for experimenting with the 1993 season, the statistical distances between the seasonal CTRL case and the decadal simulation (not plotted) are not significant at 0.05 confidence level (for TC genesis, $p = 0.08$; for lifetime maximum intensity, $p = 0.11$), while both of these free-running CAM5 cases are significantly biased from observation ($p < 0.01$, as shown in Fig. 12). For the T(0.125) case, the significant bias in TC genesis location undermines the meaningfulness of the apparent homogeneity with seasonal observation for lifetime maximum intensity. For the T(full) case, on the other hand, the previously discussed overshoot in lifetime maximum intensity denotes significant distortion to TCs' development. This statistical view suggests T(0.5), corresponding to relaxing the nudging timescale

to double that of the model, as striking a balance between ameliorating the environmental bias on the large-scale, and permitting TCs' development on the synoptic scale.

## 4 Conclusion and Discussion

In this study, we evaluate the decadal climatology of high-resolution, TC-permitting CAM5 under AMIP configurations with a focus on the WNP basin. The cold and dry biases in the large-scale environment over the Warm Pool leads to the lack of WNP TC genesis. The general lack of convection is linked to previously identified, resolution-dependent precipitation deficit (Bacmeister et al., 2014), as well as biases in the East Asian Summer Monsoon circulation (e.g., Z. Li et al., 2018). Seasonal experiments that improve the cold bias by nudging temperature over the WNP lead to improvements in moisture, precipitation, and TCs. The suite of nudging experiments confirms the importance of the large-scale environment on various aspects of convection. The statistics of WNP TC genesis and intensity development are sensitive to the choice of timescale for temperature nudging. In particular, the forcing in model physics required to restore the large-scale environment in favor of TC genesis may disrupt the intensity development.

Overall, this study shows that improving the simulated large-scale mean climate in CAM5, in this case implemented by nudging, can improve aspects of the simulation of TCs. The results suggest that improving the simulation of the mean state of thermodynamic and dynamic fields in CAM – and GCMs in general – would lead to improvements in the simulation of extreme events such as TCs. Such improvements can potentially be achieved through continued model development. At the same time, through the analysis of conventional and nudged simulations, we note some potential implications and caveats as follows.

The frequency of TC genesis, on either the global or basin scale, is known to be sensitive to subgrid-scale physical parameterizations (Zhao et al., 2012; Bacmeister et al., 2014; Zarzycki & Jablonowski, 2015), dynamical core (K. Reed et al., 2015), or choices in the tracking algorithm (Horn et al., 2014; Zarzycki & Ullrich, 2017). On the other hand, as our analysis confirms, it is the spatial pattern of TC genesis that more closely relates to the underlying large-scale mean state of the simulated climate. The analysis of the seasonal experiments further suggests that in addition to TC frequency, the spatial char-

acteristics of TC genesis and intensity development on the regional scale in relation to the environmental fields are also important for model evaluation.

As the implementation of nudging depends on the model aspect to be addressed, we argue here that the nudging of temperature serves to investigate the link between the large-scale convective environment and TCs. On the other hand, in comparison to previous studies, it is worth exploring whether spectral nudging limited to greater horizontal wavenumbers will significantly impact the results in future work. It is also worth noting that certain implementations of nudging may lead to unintended results due to responses from model physics or dynamics. One example is that, when the boundary of the horizontal nudging window is placed too close to the main development region, the temperature gradient may artificially introduce spurious vorticity. Additionally, experiments that directly nudge the specific humidity field would excessively disrupt the time evolution of model physics, effectively inhibiting any TC development. By nudging the temperature field, the response of moisture ameliorates the dry bias while partially circumventing the direct disruption.

As previously acknowledged, the direct nudging of the large-scale environment variables is an exploratory exercise rather than a solution, especially with regard to the resulting TC intensity damping. Moreover, in terms of convection and the related TC climatology, the effect of ocean coupling may lead to improvements due to better representation of air-sea fluxes (H. Li & Sriver, 2018), or degradation due to SST biases (Small et al., 2014). In the interest of high-resolution climate modeling, including those that permit TCs, one of the ongoing critical challenges is understanding the resolution- or coupling-dependent biases in the simulated mean climate, which could potentially lead to mechanistic improvements. In this context, idealized test cases specifically designed to address these issues can shed light on the physical explanations of model behavior (K. A. Reed & Jablonowski, 2012; K. A. Reed & Medeiros, 2016; A. R. Herrington & Reed, 2017; A. Herrington & Reed, 2018). Further investigation of TCs in relation to the mean climate in an idealized modeling framework may lead to additional insights, including the impact of ocean coupling (X. Wu et al., 2021).

## Acknowledgments

Wu and Reed were partially supported by U.S. Department of Energy Office of Science grants DE-SC0019459 and DE-SC0016994. The Community Earth System Model project

is supported primarily by the National Science Foundation (NSF). This material is based upon work supported by the National Center for Atmospheric Research, which is a major facility sponsored by the NSF under Cooperative Agreement No. 1852977. Computing and data storage resources, including the supercomputers Yellowstone (ark:/85065/d7wd3xhc) and Cheyenne (doi:10.5065/D6RX99HX), were provided by the Computational and Information Systems Laboratory (CISL) at NCAR. Additional high-performance computing support was provided by the Blue Waters sustained-petascale computing project also supported by the NSF and the state of Illinois. We thank Colin M. Zarzycki and Adam R. Herrington for helpful discussions. All CAM5 simulation outputs are available on CISL's Globally Accessible Data Environment. The IBTrACS dataset is obtained from the National Oceanic and Atmospheric Administration (http://www.ncdc.noaa.gov/ibtracs/). The ERA-Interim reanalysis dataset is provided by Copernicus Climate Change Service (C3S) of the European Centre for Medium-range Weather Forecast (ECMWF), available from https://www.ecmwf.int/en/forecasts/datasets/archive-datasets/reanalysis-datasets/era-interim. The MERRA-2 dataset is provided by the Global Modeling and Assimilation Office (GMAO) at NASA Goddard Space Flight Center. Both GPCP Precipitation data and Interpolated OLR data are provided by the NOAA/OAR/ESRL PSD, Boulder, Colorado, USA, from their Web site at https://www.esrl.noaa.gov/psd/.

## References

Adler, R. F., Huffman, G. J., Chang, A., Ferraro, R., Xie, P.-P., Janowiak, J., ... Bolvin, D. (2003). The version-2 global precipitation climatology project (GPCP) monthly precipitation analysis (1979–present) [Journal Article]. *Journal of hydrometeorology*, *4*(6), 1147-1167.

Bacmeister, J. T., Reed, K. A., Hannay, C., Lawrence, P., Bates, S., Truesdale, J. E., ... Levy, M. (2018). Projected changes in tropical cyclone activity under future warming scenarios using a high-resolution climate model. *Climatic Change*, *146*(3-4), 547–560.

Bacmeister, J. T., Wehner, M. F., Neale, R. B., Gettelman, A., Hannay, C., Lauritzen, P. H., ... Truesdale, J. E. (2014). Exploratory high-resolution climate simulations using the community atmosphere model (cam) [Journal Article]. *Journal of Climate*, *27*(9), 3073-3099.

Bakkensen, L. A., & Mendelsohn, R. O. (2019). Global tropical cyclone damages and

fatalities under climate change: An updated assessment. In *Hurricane risk* (pp. 179–197). Springer.

Barcikowska, M., Feser, F., Zhang, W., & Mei, W. (2017). Changes in intense tropical cyclone activity for the western north pacific during the last decades derived from a regional climate model simulation. *Climate Dynamics*, *49*(9), 2931–2949.

Berrisford, P., Kållberg, P., Kobayashi, S., Dee, D., Uppala, S., Simmons, A., ... Sato, H. (2011). Atmospheric conservation properties in era-interim. *Quarterly Journal of the Royal Meteorological Society*, *137*(659), 1381–1399.

Bister, M., & Emanuel, K. A. (2002). Low frequency variability of tropical cyclone potential intensity 1. interannual to interdecadal variability. *Journal of Geophysical Research: Atmospheres*, *107*(D24), ACL–26.

Bosilovich, M. G., Robertson, F. R., Takacs, L., Molod, A., & Mocko, D. (2017). Atmospheric water balance and variability in the merra-2 reanalysis. *Journal of Climate*, *30*(4), 1177–1196.

Bretherton, C. S., & Park, S. (2009). A new moist turbulence parameterization in the community atmosphere model. *Journal of Climate*, *22*(12), 3422–3448.

Bryan, G. H. (2008). On the computation of pseudoadiabatic entropy and equivalent potential temperature. *Monthly Weather Review*, *136*(12), 5239–5245.

Camargo, S. J., Giulivi, C. F., Sobel, A. H., Wing, A. A., Kim, D., Moon, Y., ... others (2020). Characteristics of model tropical cyclone climatology and the large-scale environment. *Journal of Climate*, *33*(11), 4463–4487.

Camargo, S. J., Robertson, A. W., Gaffney, S. J., Smyth, P., & Ghil, M. (2007). Cluster analysis of typhoon tracks. part i: General properties [Journal Article]. *Journal of Climate*, *20*(14), 3635-3653.

Choi, S.-J., & Lee, D.-K. (2016). Impact of spectral nudging on the downscaling of tropical cyclones in regional climate simulations. *Advances in Atmospheric Sciences*, *33*(6), 730–742.

Dee, D. P., Uppala, S., Simmons, A., Berrisford, P., Poli, P., Kobayashi, S., ... Bauer, P. (2011). The era-interim reanalysis: Configuration and performance of the data assimilation system [Journal Article]. *Quarterly Journal of the royal meteorological society*, *137*(656), 553-597.

Easter, R. C., Ghan, S. J., Zhang, Y., Saylor, R. D., Chapman, E. G., Laulainen,

N. S., ... Zaveri, R. A. (2004). Mirage: Model description and evaluation of aerosols and trace gases. *Journal of Geophysical Research: Atmospheres*, *109*(D20).

Emanuel, K. (2010). Tropical cyclone activity downscaled from NOAA-CIRES reanalysis, 1908–1958 [Journal Article]. *Journal of Advances in Modeling Earth Systems*, *2*(1).

Emanuel, K., & Nolan, D. S. (2004). Tropical cyclone activity and the global climate system [Conference Proceedings]. In *26th conference on hurricanes and tropical meteorolgy.*

Emanuel, K., Sundararajan, R., & Williams, J. (2008). Hurricanes and global warming: Results from downscaling ipcc ar4 simulations. *Bulletin of the American Meteorological Society*, *89*(3), 347–368.

Feser, F., & Barcikowska, M. (2012). The influence of spectral nudging on typhoon formation in regional climate models. *Environmental Research Letters*, *7*(1), 014024.

Gates, W. L. (1992, Dec). Amip: The atmospheric model intercomparison project. *Bulletin of the American Meteorological Society*, *73*(12), 1962–1970. Retrieved from `http://dx.doi.org/10.1175/1520-0477(1992)073<1962:ATAMIP>2.0.CO;2` doi: 10.1175/1520-0477(1992)073⟨1962:atamip⟩2.0.co;2

Gates, W. L., Boyle, J. S., Covey, C., Dease, C. G., Doutriaux, C. M., Drach, R. S., ... others (1999). An overview of the results of the atmospheric model intercomparison project (amip i). *Bulletin of the American Meteorological Society*, *80*(1), 29–56.

Gelaro, R., McCarty, W., Suárez, M. J., Todling, R., Molod, A., Takacs, L., ... Reichle, R. (2017). The modern-era retrospective analysis for research and applications, version 2 (merra-2) [Journal Article]. *Journal of Climate*, *30*(14), 5419-5454.

George, J. E., & Gray, W. M. (1977). Tropical cyclone recurvature and nonrecurvature as related to surrounding wind-height fields. *Journal of Applied Meteorology*, *16*(1), 34–42.

Gettelman, A., Morrison, H., & Ghan, S. J. (2008). A new two-moment bulk stratiform cloud microphysics scheme in the community atmosphere model, version 3 (cam3). part ii: Single-column and global results. *Journal of Climate*,

*21*(15), 3660–3679.

Haseler, J. (1982). *An investigation of the impact at middle and high latitudes of tropical forecast errors* (Tech. Rep. No. 31). European Centre for Medium Range Weather Forecasts.

Herrington, A., & Reed, K. (2018). An idealized test of the response of the community atmosphere model to near-grid-scale forcing across hydrostatic resolutions. *Journal of Advances in Modeling Earth Systems*, *10*(2), 560–575.

Herrington, A. R., & Reed, K. A. (2017). An explanation for the sensitivity of the mean state of the community atmosphere model to horizontal resolution on aquaplanets. *Journal of Climate*, *30*(13), 4781–4797.

Horn, M., Walsh, K., Zhao, M., Camargo, S. J., Scoccimarro, E., Murakami, H., ... others (2014). Tracking scheme dependence of simulated tropical cyclone response to idealized climate simulations. *Journal of climate*, *27*(24), 9197–9213.

Klinker, E. (1990). Investigation of systematic errors by relaxation experiments. *Quarterly Journal of the Royal Meteorological Society*, *116*(493), 573–594.

Knapp, K. R., Kruk, M. C., Levinson, D. H., Diamond, H. J., & Neumann, C. J. (2010). The international best track archive for climate stewardship (ibtracs) unifying tropical cyclone data [Journal Article]. *Bulletin of the American Meteorological Society*, *91*(3), 363-376.

Knutson, T. R., Sirutis, J. J., Garner, S. T., Held, I. M., & Tuleya, R. E. (2007). Simulation of the recent multidecadal increase of atlantic hurricane activity using an 18-km-grid regional model. *Bulletin of the American Meteorological Society*, *88*(10), 1549–1565.

Lee, H. (2014). Climate algorithm theoretical basis document (c-atbd): Outgoing longwave radiation (olr)-daily. noaa's climate data record (cdr) program. *Technical Report CDRP-ATBD-0526*, 46.

Li, H., & Sriver, R. L. (2018). Tropical cyclone activity in the high-resolution community earth system model and the impact of ocean coupling [Journal Article]. *Journal of Advances in Modeling Earth Systems*, *10*(1), 165-186.

Li, Z., He, P., Zhu, J., Chen, H., Zeng, G., & Deng, W. (2018). Improving the simulation of east asian summer monsoon with mesoscale enhancement in an agcm. *Climate Dynamics*, 1–12.

Moon, J., Cha, D.-H., Lee, M., & Kim, J. (2018). Impact of spectral nudging on real-time tropical cyclone forecast. *Journal of Geophysical Research: Atmospheres*, *123*(22), 12–647.

Murakami, H., Vecchi, G. A., Underwood, S., Delworth, T. L., Wittenberg, A. T., Anderson, W. G., ... Lin, S.-J. (2015). Simulation and prediction of category 4 and 5 hurricanes in the high-resolution GFDL hiflor coupled climate model [Journal Article]. *Journal of Climate*, *28*(23), 9058-9079.

Murakami, H., Wang, B., & Kitoh, A. (2011). Future change of western north pacific typhoons: Projections by a 20-km-mesh global atmospheric model [Journal Article]. *Journal of Climate*, *24*(4), 1154-1169.

NCAR. (2017). *Cam6 user's guide.* Retrieved 06-28-2019, from `https://ncar.github.io/CAM/doc/build/html/users_guide/physics-modifications-via-the-namelist.html`

Neale, R. B., Chen, C.-C., Gettelman, A., Lauritzen, P. H., Park, S., Williamson, D. L., ... Lamarque, J.-F. (2012). Description of the NCAR community atmosphere model (CAM 5.0) [Journal Article]. *NCAR Tech. Note NCAR/TN-486+ STR*.

Ogata, T., Mizuta, R., Adachi, Y., Murakami, H., & Ose, T. (2015). Effect of air-sea coupling on the frequency distribution of intense tropical cyclones over the northwestern Pacific [Journal Article]. *Geophysical Research Letters*, *42*(23), 10,415–10,421.

Park, S., & Bretherton, C. S. (2009). The university of washington shallow convection and moist turbulence schemes and their impact on climate simulations with the community atmosphere model. *Journal of Climate*, *22*(12), 3449–3469.

Reed, K., Bacmeister, J., Rosenbloom, N., Wehner, M., Bates, S., Lauritzen, P., ... Hannay, C. (2015). Impact of the dynamical core on the direct simulation of tropical cyclones in a high-resolution global model [Journal Article]. *Geophysical Research Letters*, *42*(9), 3603-3608.

Reed, K. A., Bacmeister, J. T., Huff, J. J. A., Wu, X., Bates, S. C., & Rosenbloom, N. A. (2019). Exploring the impact of dust on North Atlantic hurricanes in a high-resolution climate model. *Geophysical Research Letters*, *46*(2), 1105–1112.

Reed, K. A., & Jablonowski, C. (2011). Impact of physical parameterizations on idealized tropical cyclones in the community atmosphere model. *Geophysical Research Letters*, *38*(4), 1-5.

Reed, K. A., & Jablonowski, C. (2012). Idealized tropical cyclone simulations of intermediate complexity: A test case for AGCMs. *Journal of Advances in Modeling Earth Systems*, *4*(2).

Reed, K. A., & Medeiros, B. (2016). A reduced complexity framework to bridge the gap between agcms and cloud-resolving models. *Geophysical Research Letters*, *43*(2), 860–866.

Roberts, M. J., Camp, J., Seddon, J., Vidale, P. L., Hodges, K., Vanniere, B., ... others (2020). Impact of model resolution on tropical cyclone simulation using the highresmip–primavera multimodel ensemble. *Journal of Climate*, *33*(7), 2557–2583.

Sadler, J. C. (1976). *Tropical cyclone initiation by the tropical upper tropospheric trough* (Tech. Rep.). HAWAII UNIV HONOLULU DEPT OF METEOROLOGY.

Scoccimarro, E., Fogli, P. G., Reed, K. A., Gualdi, S., Masina, S., & Navarra, A. (2017). Tropical cyclone interaction with the ocean: The role of high-frequency (subdaily) coupled processes [Journal Article]. *Journal of Climate*, *30*(1), 145-162.

Shaevitz, D. A., Camargo, S. J., Sobel, A. H., Jonas, J. A., Kim, D., Kumar, A., ... Reed, K. A. (2014). Characteristics of tropical cyclones in high-resolution models in the present climate [Journal Article]. *Journal of Advances in Modeling Earth Systems*, *6*(4), 1154-1172.

Small, R. J., Bacmeister, J., Bailey, D., Baker, A., Bishop, S., Bryan, F., ... others (2014). A new synoptic scale resolving global climate simulation using the community earth system model. *Journal of Advances in Modeling Earth Systems*, *6*(4), 1065–1094.

Sobel, A. H., & Camargo, S. J. (2005). Influence of western north pacific tropical cyclones on their large-scale environment [Journal Article]. *Journal of the atmospheric sciences*, *62*(9), 3396-3407.

Stansfield, A. M., Reed, K. A., Zarzycki, C. M., Ullrich, P. A., & Chavas, D. R. (2020). Assessing tropical cyclones' contribution to precipitation over the

eastern united states and sensitivity to the variable-resolution domain extent. *Journal of Hydrometeorology*, *21*(7), 1425–1445.

Ullrich, P. A., & Zarzycki, C. M. (2016). Tempestextremes v1. 0: A framework for scale-insensitive pointwise feature tracking on unstructured grids. *Geosci. Model Dev. Discuss*.

von Storch, H., Langenberg, H., & Feser, F. (2000). A spectral nudging technique for dynamical downscaling purposes. *Monthly weather review*, *128*(10), 3664–3673.

Walsh, K. J., Camargo, S. J., Vecchi, G. A., Daloz, A. S., Elsner, J., Emanuel, K., ... Patricola, C. (2015). Hurricanes and climate: the US CLIVAR working group on hurricanes [Journal Article]. *Bulletin of the American Meteorological Society*, *96*(6), 997-1017.

Wang, H., Wang, Y., & Xu, H. (2013). Improving simulation of a tropical cyclone using dynamical initialization and large-scale spectral nudging: A case study of typhoon megi (2010). *Acta Meteorologica Sinica*, *27*(4), 455–475.

Wehner, M. F., Reed, K. A., Li, F., Bacmeister, J., Chen, C., Paciorek, C., ... Gettelman, A. (2014). The effect of horizontal resolution on simulation quality in the community atmospheric model, cam5. 1 [Journal Article]. *Journal of Advances in Modeling Earth Systems*, *6*(4), 980-997.

Wehner, M. F., Reed, K. A., & Zarzycki, C. M. (2017). High-resolution multi-decadal simulation of tropical cyclones. In *Hurricanes and climate change* (pp. 187–211). Springer.

Wilks, D. S. (2011). *Statistical methods in the atmospheric sciences* (Vol. 100) [Book]. Academic press.

Wu, L., Chou, C., Chen, C.-T., Huang, R., Knutson, T. R., Sirutis, J. J., ... Feng, Y.-C. (2014). Simulations of the present and late-twenty-first-century western north pacific tropical cyclone activity using a regional model. *Journal of Climate*, *27*(9), 3405–3424.

Wu, L., Wen, Z., Huang, R., & Wu, R. (2012). Possible linkage between the monsoon trough variability and the tropical cyclone activity over the western north pacific. *Monthly Weather Review*, *140*(1), 140–150.

Wu, X., Reed, K. A., Wolfe, C. L., Marques, G. M., Bachman, S. D., & Bryan, F. O. (2021). Coupled Aqua and Ridge planets in the Community Earth System

Model. *Journal of Advances in Modeling Earth Systems*, e2020MS002418. doi: 10.1029/2020MS002418

Yesubabu, V., Srinivas, C., Ramakrishna, S., & Prasad, K. H. (2014). Impact of period and timescale of fdda analysis nudging on the numerical simulation of tropical cyclones in the bay of bengal. *Natural hazards*, *74*(3), 2109–2128.

Zarzycki, C. M. (2016). Tropical cyclone intensity errors associated with lack of two-way ocean coupling in high-resolution global simulations [Journal Article]. *Journal of Climate*, *29*(23), 8589-8610.

Zarzycki, C. M., & Jablonowski, C. (2015). Experimental tropical cyclone forecasts using a variable-resolution global model. *Monthly Weather Review*, *143*(10), 4012–4037.

Zarzycki, C. M., & Ullrich, P. A. (2017). Assessing sensitivities in algorithmic detection of tropical cyclones in climate data. *Geophysical Research Letters*, *44*(2), 1141–1149.

Zhang, G. J., & McFarlane, N. A. (1995). Sensitivity of climate simulations to the parameterization of cumulus convection in the Canadian Climate Centre general circulation model. *Atmosphere-ocean*, *33*(3), 407–446.

Zhang, W., Leung, Y., & Chan, J. C. (2013a). The analysis of tropical cyclone tracks in the western north pacific through data mining. part ii: Tropical cyclone landfall. *Journal of Applied Meteorology and Climatology*, *52*(6), 1417–1432.

Zhang, W., Leung, Y., & Chan, J. C. (2013b). The analysis of tropical cyclone tracks in the western north pacific through data mining. part i: Tropical cyclone recurvature. *Journal of Applied Meteorology and Climatology*, *52*(6), 1394–1416.

Zhao, M., Held, I. M., & Lin, S.-J. (2012). Some counterintuitive dependencies of tropical cyclone frequency on parameters in a gcm. *Journal of the Atmospheric Sciences*, *69*(7), 2272–2283.

Zhao, M., Held, I. M., Lin, S.-J., & Vecchi, G. A. (2009, Dec). Simulations of global hurricane climatology, interannual variability, and response to global warming using a 50-km resolution gcm. *Journal of Climate*, *22*(24), 6653–6678. Retrieved from `http://dx.doi.org/10.1175/2009JCLI3049.1` doi: 10.1175/2009jcli3049.1

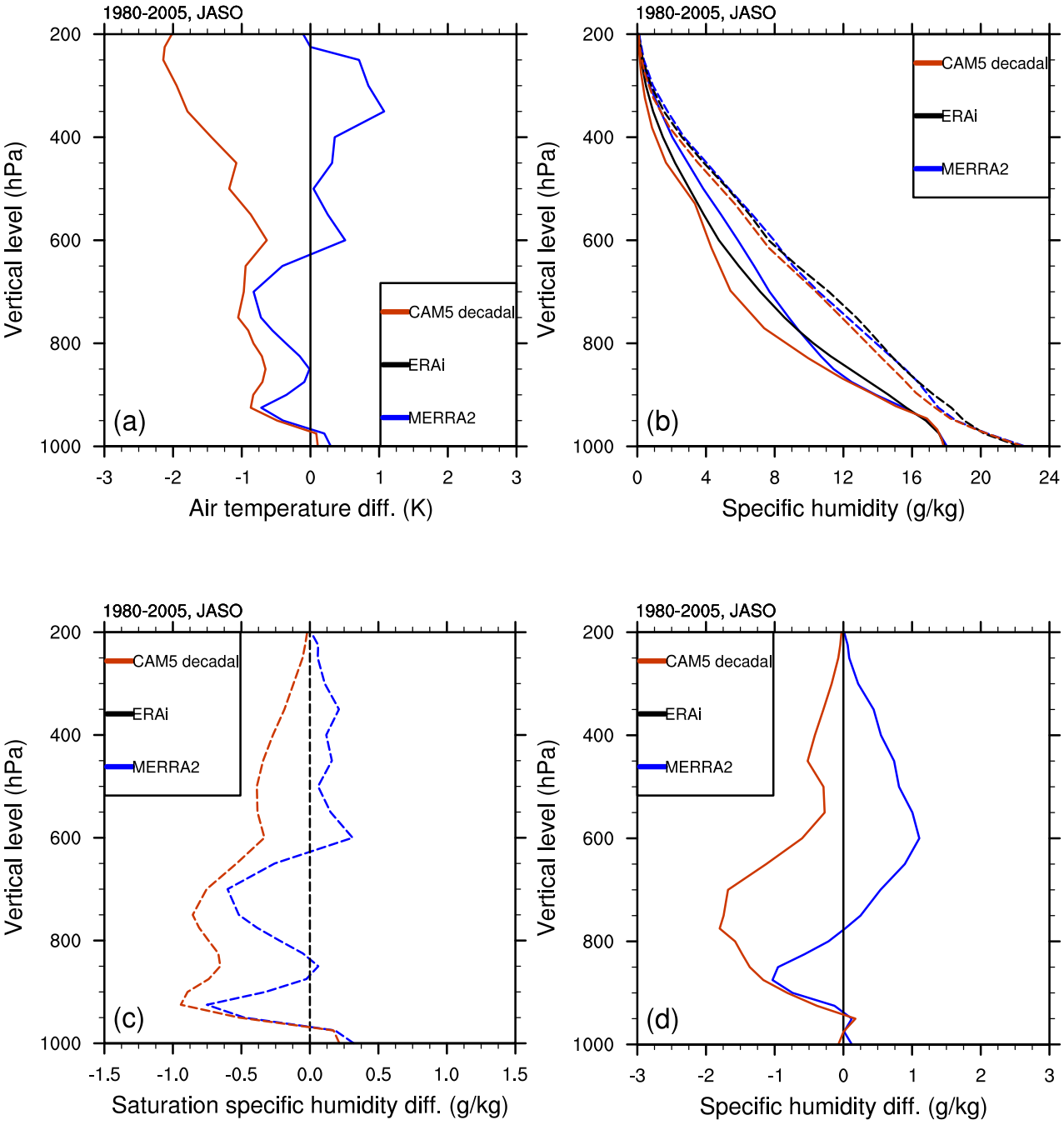


**Figure 5.** (a): Differences from ERA-Interim in the vertical profiles of temperature, of CAM5 decadal simulation and MERRA2, respectively; (b): Vertical profiles of specific humidity and saturation specific humidity of CAM5 decadal simulation and the two reanalyses; (c): as (a), but for saturation specific humidity; (d): as (a), but for specific humidity. All profiles are averaged over 10-20°N, 130-150°E (the blue boxes in Fig. 3), July-October 1980-2005. In (b), (c), and (d), solid lines represent specific humidity, and dashed lines represent saturation specific humidity.

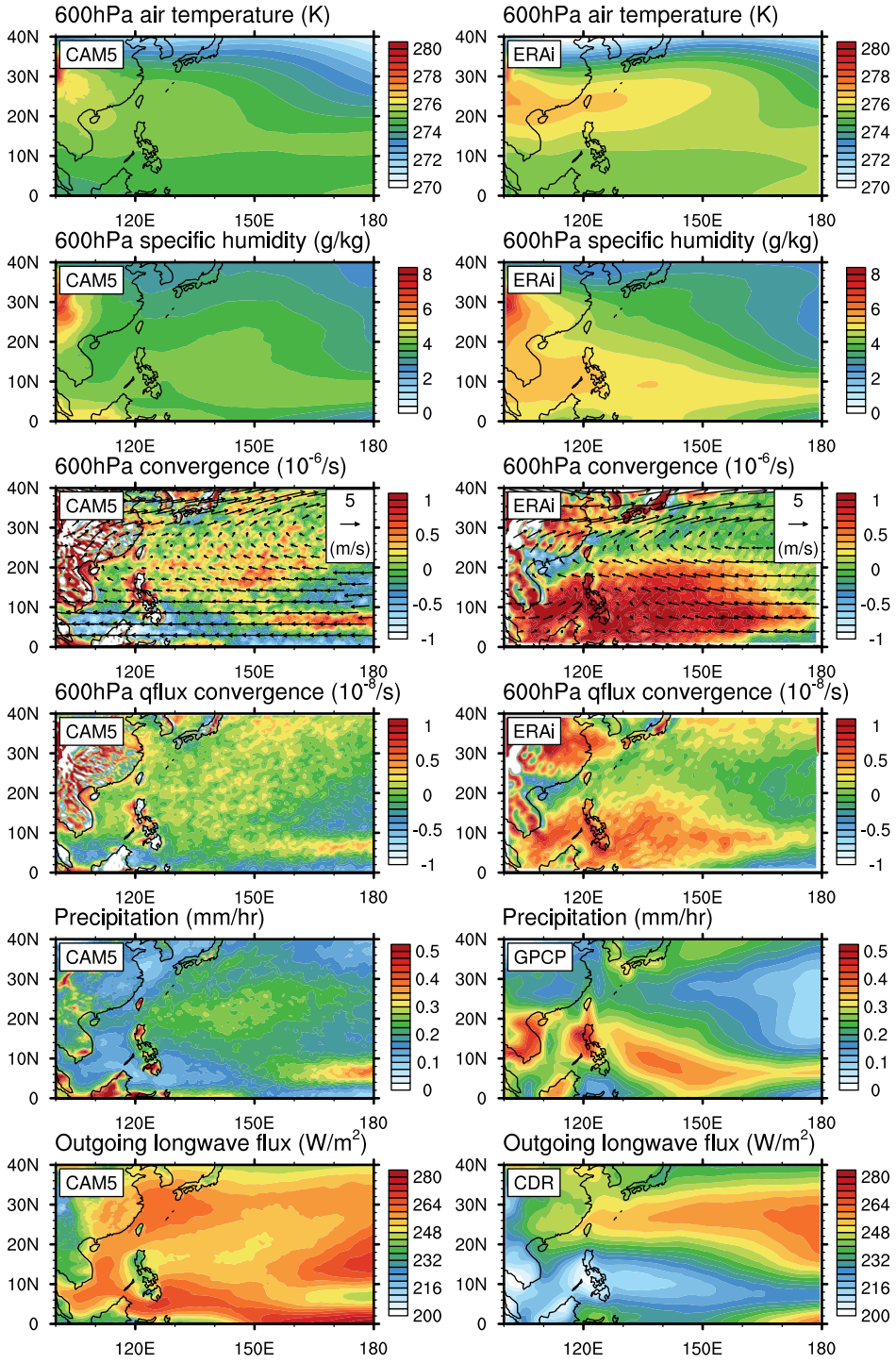


**Figure 6.** Large-scale environments in CAM5 and observation, July-October 1980-2005: 600 hPa temperature, specific humidity, wind (vectors) and horizontal convergence (shaded contours), horizontal convergence of moisture flux, precipitation, and outgoing longwave radiation.

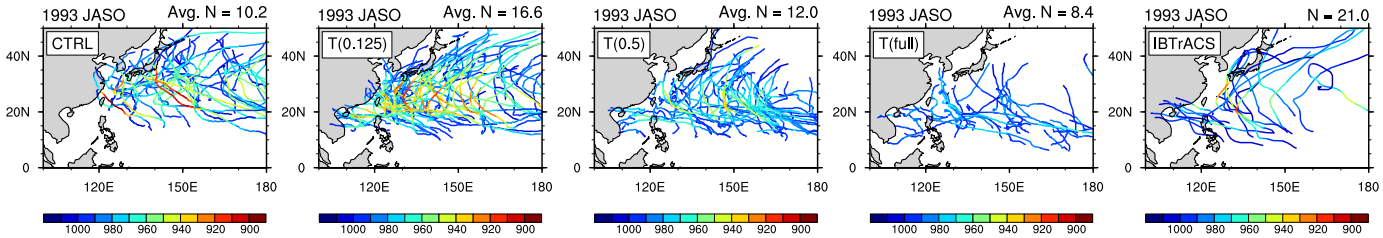


**Figure 7.** WNP TC tracks and intensity from observation and CAM5 seasonal experiments (see Section 2.2 for details), July-October 1993. In the seasonal experiments, all tracks from the five ensemble members are shown, while the number of TCs is averaged, shown in the upper right corner.

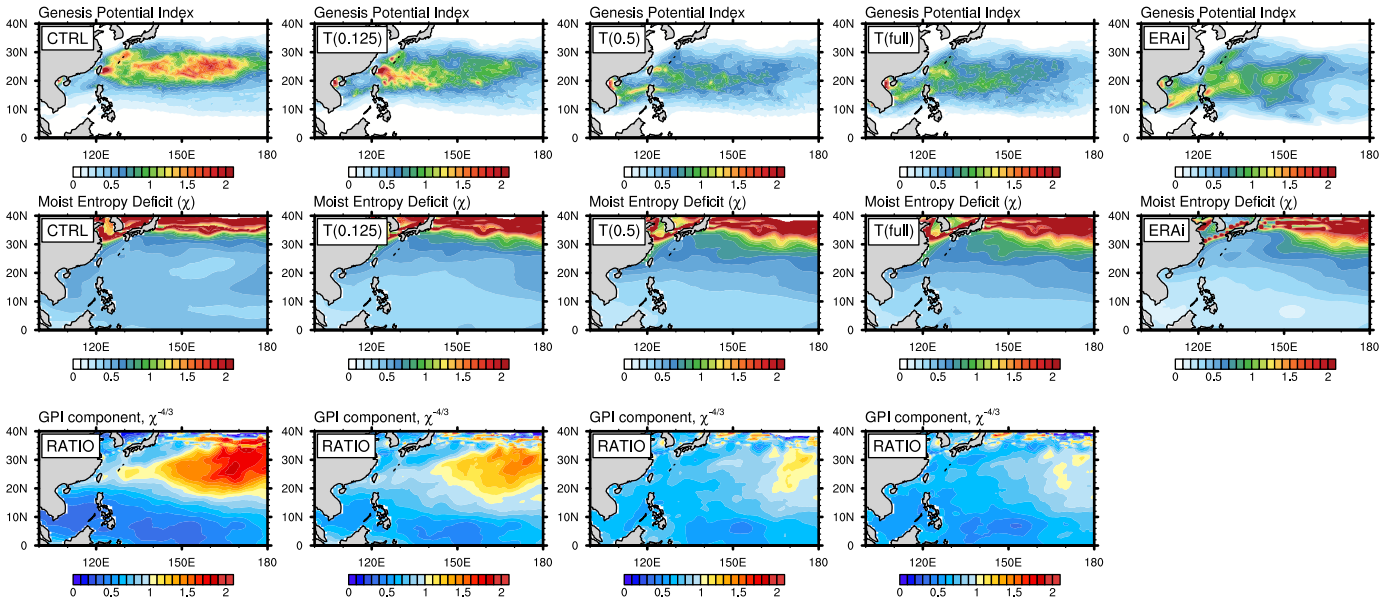


**Figure 8.** GPI from observation and CAM5 seasonal experiments, July-October 1993 as in Fig. 3, and the moist entropy deficit component with its contribution to GPI bias as in Fig. 4.

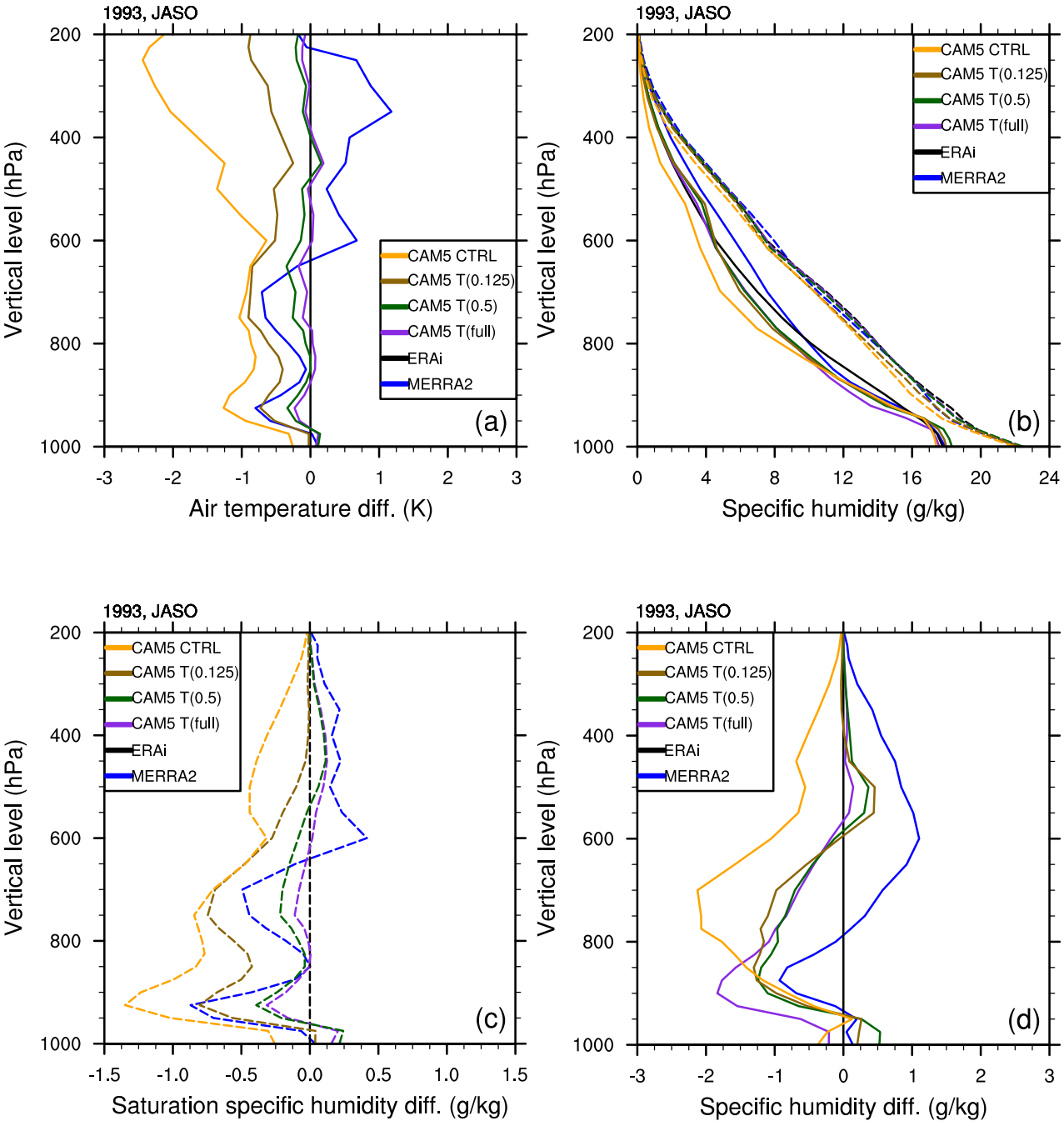


**Figure 9.** Same as Fig. 5, but for CAM5 seasonal experiments (ensemble average for each case of experiment) and the two reanalyses, July-October 1993.

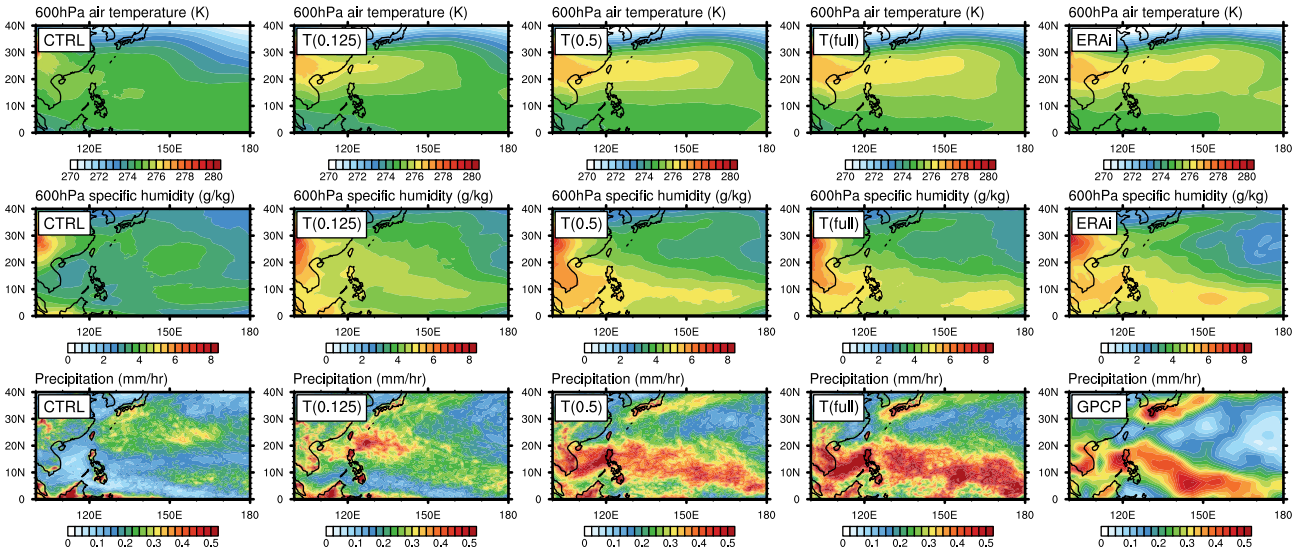


**Figure 10.** Large-scale environments in CAM5 seasonal experiments and observation, averaged over July-October 1993: 600 hPa temperature, specific humidity, and precipitation.

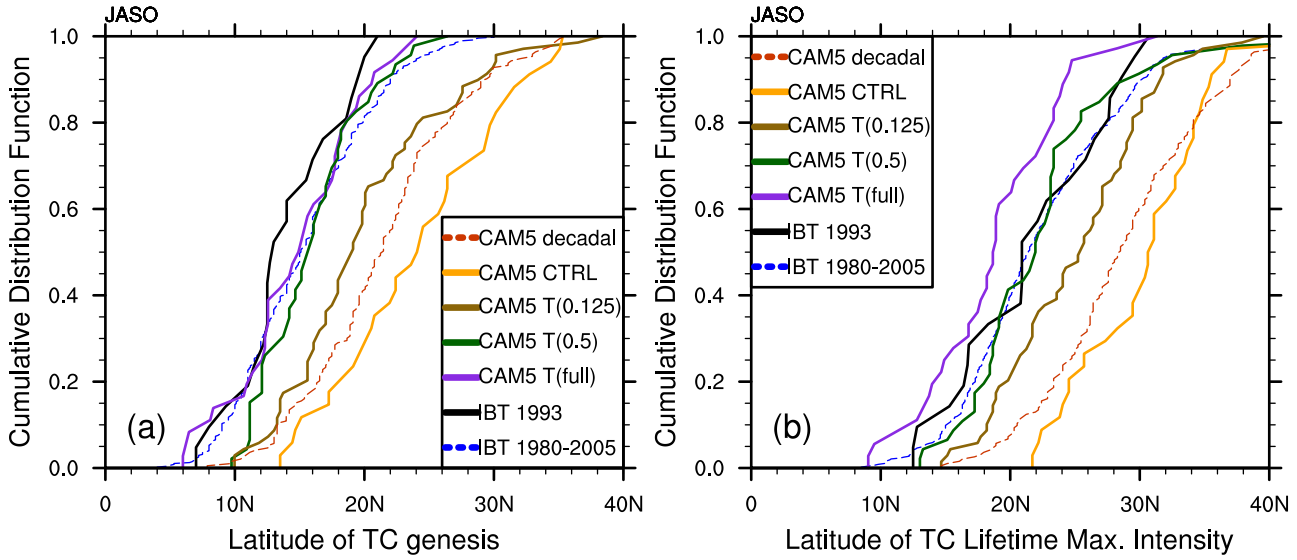


**Figure 11.** Cumulative distribution functions for the latitude of (a) TC genesis, and (b) lifetime maximum intensity.

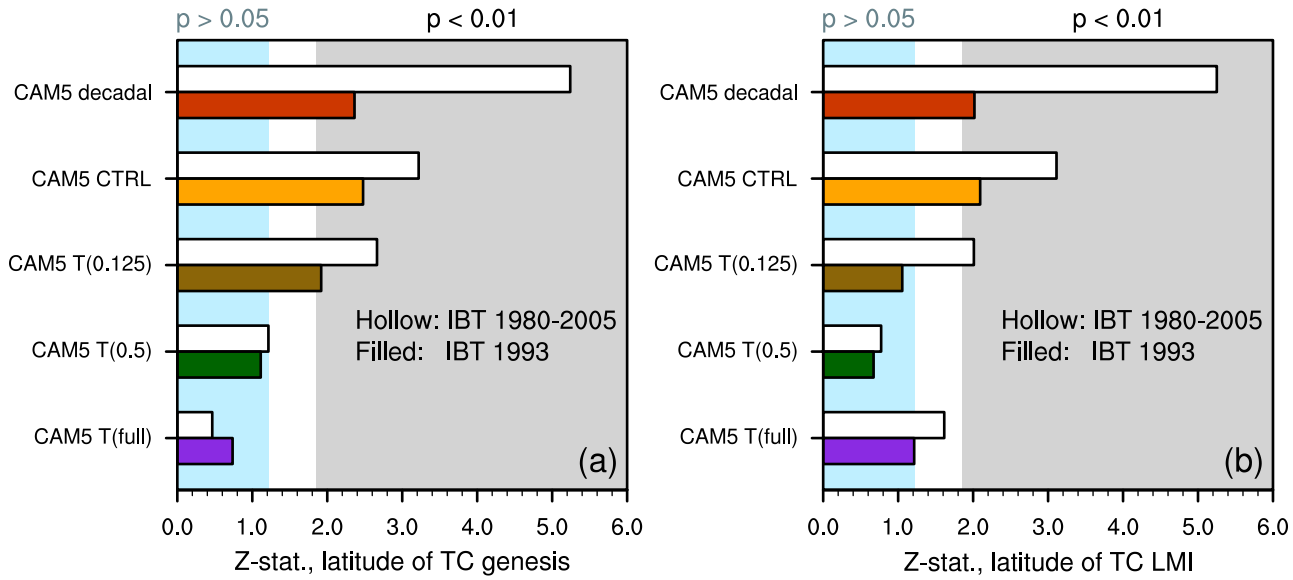


**Figure 12.** The Z-statistics from the two-sided Kolmogorov-Smirnov test (see Section 2.3 for details) between the CAM5 cases and observed decadal and seasonal records. Higher values of Z-statistics correspond to higher confidence levels for rejecting the null hypothesis of homogeneity, as indicated by the two shaded zones in the background. Light blue zone: The null hypothesis cannot be rejected at 0.05 confidence level; Light gray zone: The null hypothesis can be rejected at 0.01 confidence level.